CO_2 Capture from Dry Flue Gas by Vacuum Swing Adsorption: A Pilot Plant Study

Shreenath Krishnamurthy and Vemula Rama Rao
Dept. of Chemical and Biomolecular Engineering, National University of Singapore, Singapore 117585

Sathishkumar Guntuka and Paul Sharratt
Institute of Chemical and Engineering Sciences, Singapore 627833

Reza Haghpanah, Arvind Rajendran, and Mohammad Amanullah
School of Chemical and Biomedical Engineering, Nanyang Technological University, Singapore 637459

Iftekhar A. Karimi and Shamsuzzaman Farooq
Dept. of Chemical and Biomolecular Engineering, National University of Singapore, Singapore 117585

DOI 10.1002/aic.14435
Published online March 20, 2014 in Wiley Online Library (wileyonlinelibrary.com)

The capture and concentration of CO_2 from a dry flue gas by vacuum swing adsorption (VSA) has been experimentally demonstrated in a pilot plant. The pilot plant has the provision for using two coupled columns that are each packed with approximately 41 kg of Zeochem zeolite 13X. Breakthrough experiments were first carried out by perturbing a N_2 saturated bed with 15% CO_2 and 85% N_2 feed, which is representative of a dry flue gas from coal-fired power plants. The breakthrough results showed long plateaus in temperature profiles confirming a near adiabatic behavior. In the process study, a basic four-step vacuum swing adsorption (VSA) cycle comprising the following steps: pressurization with feed, adsorption, forward blowdown, and reverse evacuation was investigated first. In the absence of any coupling among the steps, a single bed was used. With this cycle configuration, CO_2 was concentrated to 95.9 ± 1% with a recovery of 86.4 ± 5.6%. To improve the process performance, a four-step cycle with light product pressurization (LPP) using two beds was investigated. This cycle was able to achieve 94.8 ± 1% purity and 89.7 ± 5.6% recovery. The Department of Energy requirements are 95% purity and 90% recovery. The proposed underlying physics of performance improvement of the four-step cycle with LPP has also been experimentally validated. The pilot plant results were then used for detailed validation of a one-dimensional, nonisothermal, and nonisobaric model. Both transient profiles of various measured variables and cyclic steady state performance results were compared with the model predictions, and they were in good agreement. The energy consumptions in the pilot plant experiments were 339–583 ± 36.7 kWh tonne^{-1} CO_2 captured and they were significantly different from the theoretical power consumptions obtained from isentropic compression calculations. The productivities were 0.87–1.4 ± 0.07 tonne CO_2 m^{-3} adsorbent day^{-1}. The results from our pilot plant were also compared with available results from other pilot plant studies on CO_2 capture from flue gas.
 AIChE J, 60: 1830–1842, 2014

This work is dedicated to the memory of Dr PK Wong who did not live to see the completion of CCU TSRP that he initiated and managed for the most part of the program's duration.

Keywords: CO_2 capture, zeolite 13X, vacuum swing adsorption, light product pressurization, modeling and simulation, pilot plant demonstration

Introduction

The increase in CO_2 concentration in the earth's atmosphere due to anthropogenic activities has been acknowledged as the major cause for global warming. Bulk of the CO_2 emissions come from power plants using nonrenewable energy sources like coal.[1] Thus, various options are being explored to reduce CO_2 emissions from these sources. One possible way is to completely substitute fossil fuels with renewable sources of energy. However, it has been estimated that coal will still supply 28% of the world's energy demands in 2030.[2] Therefore,

This article is based on a contribution that was identified by Holly M. Krutka (ADA Environmental Solutions) and Joeri Denayer (Vrije Universiteit Brussel) as the Best Presentation in the session "CO_2 Capture by Adsorption Process and Storage" of the 2012 AIChE Annual Meeting in Pittsburgh, PA.

Additional Supporting Information may be found in the online version of this article.

Current address of Arvind Rajendran: Dept. of Chemical and Materials Engineering, University of Alberta, Edmonton, Alberta T6G2V4, Canada

Correspondence concerning this article should be addressed to S. Farooq at chesf@nus.edu.sg.

the interim measure advocated for reducing CO_2 emissions is its capture and storage.[1] This is expected to be achieved by retrofitting existing plants and by constructing new ones with a capture plant. Postcombustion flue gas from coal-fired power plants contains 12–15 mol % CO_2 at atmospheric pressure. The capture units are expected to concentrate the CO_2 from flue gas with purity and recovery exceeding 95 and 90%, respectively.[3] The most mature technology for postcombustion carbon capture is absorption using amine-based liquid solvents.[4,5] But this technology is energy intensive due to the high energy requirements for solvent regeneration.[6] Therefore, alternate technologies are being explored and adsorption, using solid sorbents, is one promising alternative.[5,7–9]

Cyclic adsorption processes alter between adsorption and desorption modes of operation. Based on the intensive variable that is cycled, the adsorption processes are broadly classified as pressure swing (PSA) or temperature swing adsorption (TSA) processes. If the cycle switches between adsorption at atmospheric pressure and desorption at vacuum, then it is called vacuum swing adsorption (VSA). Pressure vacuum swing adsorption (PVSA) cycles have adsorption step at pressures above atmospheric and desorption under vacuum.

Adsorption-based processes for gas separations have extensively been studied and several industrial applications like air separation,[10,11] hydrogen purification,[12,13] hydrocarbon separation,[14] and air drying[15] are in existence. Several PSA/VSA cycles specific to CO_2 capture have also been studied in the literature.[16] An early experimental work on carbon capture was by Ishibashi et al.[17] who used a two-stage process in a pilot plant to capture CO_2 from a power plant flue gas with Ca-X zeolite. In the first stage, a PSA-TSA process was studied, where the adsorption took place at atmospheric pressure and desorption was carried out by simultaneous heating and depressurization. In the first stage, they were able to concentrate the flue gas stream to 60 mol % CO_2. In the second stage, using a PSA process, 90 mol % CO_2 recovery with 99% purity was achieved. The overall energy consumption was 560 kWh tonne^{-1} CO_2 captured.

Cho et al.[18] studied a two-stage PSA process with zeolite 13X for a flue gas containing 10.5 mol % CO_2. The major steps involved in their process were adsorption, pressure equalization, blowdown, low pressure purge, and feed pressurization. Their first stage gave an enriched stream containing 63.2 mol % CO_2 with a recovery of 92.4%. This stream was then concentrated to 99% in the second stage with 88% recovery. The overall recovery of the process was 80% and experimental power consumption was 1.26–1.52 kWh Nm^{-3} CO_2 (641.5–770 kWh tonne^{-1} CO_2 captured).

Liu et al.[19] used zeolite 5A to study the capture and concentration of CO_2 from a dry flue gas using a three-bed, seven-step PVSA process. The major steps involved in their process were pressurization, high pressure adsorption, cocurrent depressurization, heavy product rinse, blowdown, purge, and pressure equalization. With this cycle configuration, 79% of the CO_2 was captured with 85% purity. The overall energy consumption of this process was 2.37 MJ kg^{-1} of CO_2 captured (656 kWh tonne^{-1} CO_2 captured).

Lu et al.[20] studied the capture of CO_2 from a dry flue gas in a three-bed, seven-step, single-stage process which involved adsorption, blowdown, evacuation, purge, rinse, and pressure equalization steps. The adsorbent used in their study was zeolite 13X. The best result achieved from this cycle was 85% purity and 80% recovery with an energy consumption of 440 kWh tonne^{-1} CO_2 capture. In a follow up work,[21] they used a two-stage PVSA process. The first stage, comprising three beds, used a five-step VSA process consisting of the following steps: pressurization, adsorption, rinse, blowdown, and purge. With 13X zeolite as the adsorbent, this stage was able to achieve a CO_2 purity of 73–82% and a recovery of 85–95%. In the second stage, using a two-bed, six-step VSA process with activated carbon, CO_2 was concentrated to 95% with an overall recovery of 90%. The total energy consumption of this cycle configuration was 675 kWh tonne^{-1} CO_2.

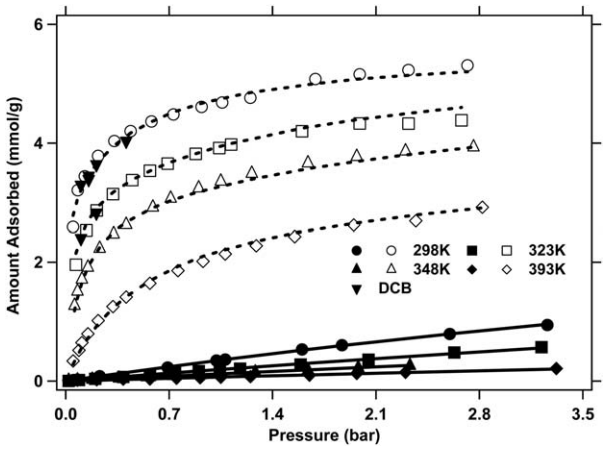

Figure 1. CO_2 (open symbols) and N_2 (closed symbols) equilibrium data in Zeochem zeolite 13X from gravimetry and dynamic column breakthrough experiments.

The lines denote the dual-site Langmuir model fits.

Webley and coworkers[22,23] have demonstrated the capture of CO_2 with six-step and nine-step VSA processes from a feed containing 12% CO_2 and 88% N_2 using zeolite 13X as the adsorbent. With the nine-step process, 95% purity and 85% recovery were achieved, and the energy consumption was 387 kWh tonne^{-1} CO_2. In the six-step process, 85% of CO_2 was captured with a purity of 83%. The overall energy consumption of this process was 249 kWh tonne^{-1} CO_2.

The main objective of the current work is to communicate the results from a pilot-scale study on CO_2 capture from dry flue gas containing 15% CO_2 in balance nitrogen on 13X zeolite—the current benchmark adsorbent for CO_2 capture and concentration. The main contributions of this communication are:

1. Pilot-scale demonstration of capture and concentration of CO_2 from a dry flue gas containing 15 mol % CO_2 to a 95% CO_2 with 90% recovery in a single stage.

2. Modeling of four-step cycle and its light product pressurization (LPP) variant along with the analysis of CO_2 purity, recovery, productivity, and energy consumption.

3. Direct experimental validation of the underlying physics contributing to the performance improvement of the four-step cycle with LPP.

4. Comparison of the measured energy consumption values from direct measurements with those from conventional isentropic and adiabatic compression calculations.

Adsorption Equilibrium and Kinetics

As the first step, single component isotherms of CO_2 and N_2 in Zeochem zeolite 13X were obtained using the RUBOTHERM gravimetric apparatus and the adsorption isotherms

Table 1. Adsorption Isotherm Parameters of CO_2 and N_2 in Zeochem zeolite 13X

Parameter	CO_2	N_2
q_{sb} (mol m^{-3})	3489.44	6613.55
b_0 (m^3 mol^{-1})	8.65×10^{-7}	2.50×10^{-6}
ΔU_b (kJ mol^{-1})	−36.64	−15.82
q_{sd} (mol m^{-3})	2872.35	0
d_0 (m^3 mol^{-1})	2.63×10^{-8}	0
ΔU_d (kJ mol^{-1})	−35.70	0

are shown in Figure 1. The isotherm data were then fitted to a dual-site Langmuir model,[23] which is of the form

$$q_i^* = \frac{q_{sb,i} b_i C_i}{1 + b_i C_i} + \frac{q_{sd,i} d_i C_i}{1 + d_i C_i} \quad (1)$$

$$b_i = b_{0i} e^{\frac{-\Delta U_{b,i}}{RT}} \quad (2)$$

$$d_i = d_{0i} e^{\frac{-\Delta U_{d,i}}{RT}} \quad (3)$$

The model parameters reported earlier by Haghpanah et al.[9] are reproduced in Table 1 for the sake of completeness. Dynamic column breakthrough (DCB) experiments were then performed to confirm the single component gravimetric data and validate the extended dual-site Langmuir model for binary adsorption. Equilibrium data obtained from mass balances of the single component DCB runs are included in Figure 1, showing good agreement with the gravimetric data. The binary equilibrium data, similarly extracted from the mass balance of the binary breakthrough runs, were also in good agreement with the predictions of the positively correlated extended dual-site Langmuir model,[24] using single component parameters, as may be seen from Figure 2. The breakthrough experiments for

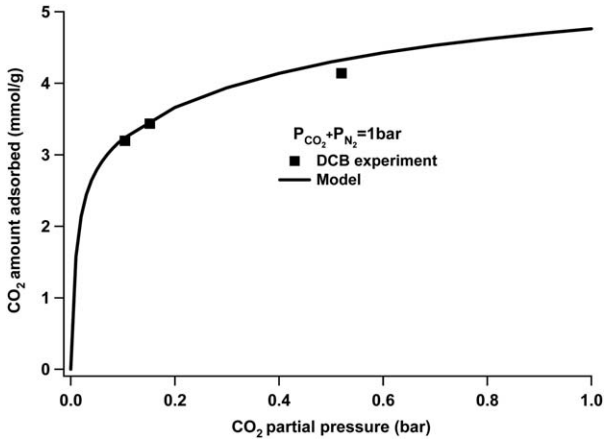

Figure 2. Validation of the positively correlated extended dual-site Langmuir model for binary adsorption.

The experimental results are from binary dynamic column breakthrough experiments.

binary equilibrium validation are detailed in the Supplementary Information.

In addition to the adsorption equilibrium, information about the mass transfer kinetics is also necessary to design an effective adsorption process. Hu et al.[25] studied the diffusion mechanism of CO_2 in 13X by zero-length column technique with bead sizes of 1.96 and 3.8 mm and it was found that adsorption of CO_2 was macropore molecular diffusion controlled with contribution from Knudsen diffusion in the low pressure regime. Giesy et al.[26] measured the mass transfer rate for CO_2 adsorption on zeolite 13X using frequency

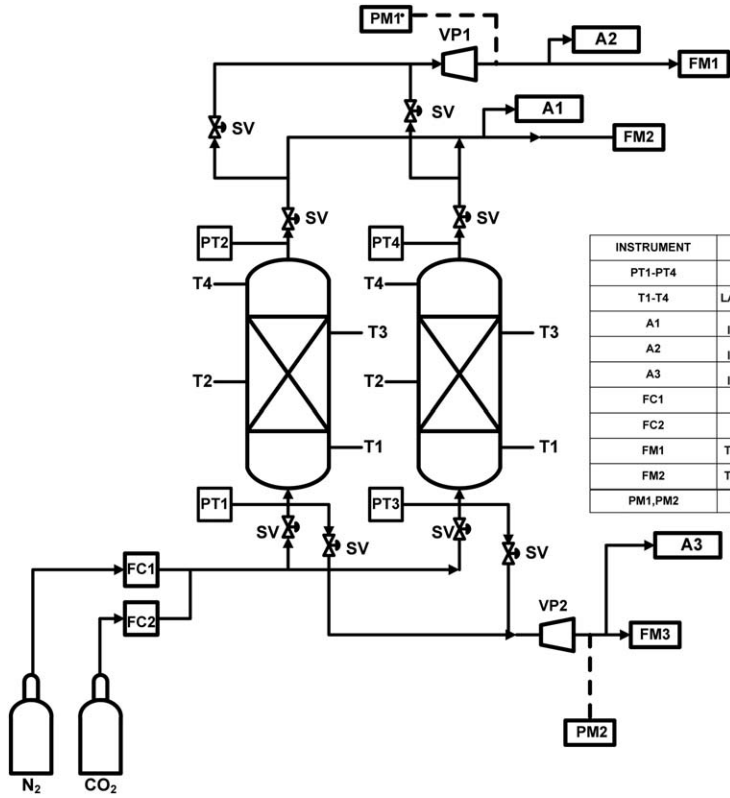

INSTRUMENT	BRAND	RANGE	MANUFACTURER REPORTED ERROR
PT1-PT4	GE UNIK 5000	0-10 bar	±0.04% FS
T1-T4	LAB FACILITY PT-100	-100 to 450°C	±1°C
A1	QUANTEK INSTRUMENTS 906	0-5%	±1% FS
A2	QUANTEK INSTRUMENTS 906	0-50%	±1% FS
A3	QUANTEK INSTRUMENTS 906	0-100%	±1% FS
FC1	BROOKS 5850E	0-1250 SLPM	±1% FS
FC2	BROOKS 5850E	0-250 SLPM	±1% FS
FM1	TELEDYNE HFM 305	0-1800 SLPM	±1% FS
FM2	TELEDYNE HFM 200	0-250 SLPM	±1% FS
PM1,PM2	LUTRON DW 6093	10-600 V	±0.5%

Figure 3. Schematic of the pilot plant.

SV-solenoid valve, PT-pressure transducer, FM-flow meter, FC-flow controller, A1-A3-CO_2 analyzers, T1-T4-thermocouples, VP1 and VP2-vacuum pumps. The instrument specifications are also listed here.

response technique for pressures of 0.125, 0.5, and 1 bar and had found that that mass transfer kinetics was well described by the Knudsen diffusion mechanism. In view of these studies, macropore molecular diffusion control was assumed for adsorption kinetics in the present study.

Description of the Pilot Plant Setup

A simplified schematic of the pilot plant is shown in Figure 3 along with the instrument specifications. Some representative snapshots of the pilot plant are shown in Figure S2 in the Supplementary Information. The pilot plant is equipped with two identical adsorption columns with 0.3 m internal diameter and a wall thickness of 0.02 m. Each of the two columns was packed up to 0.867 m of height with ~41 kg of adsorbent (bed voidage of 0.428 and particle size in the range 1.6–2.6 mm). Both columns were fitted with custom-built distributors to ensure that the feed was well distributed in the radial direction. The columns were mounted onto the main panel carrying the piping, valves, and pressure sensors. Two mass flow controllers were used to supply CO_2 and N_2 at the desired flow rates. Thermocouples were inserted along the column at four axial positions (0.043, 0.28, 0.51, and 0.75 m from the bottom distributor plate) to measure transient temperature profiles during the experiments. The pressures at the inlet and outlet of the columns were measured using the pressure transducers located at both ends of the column. The exit CO_2 compositions were analyzed using different infrared CO_2 analyzers for the high pressure adsorption, blowdown, and evacuation steps, respectively. Two vacuum pumps (EVISA E-65 and E-100) were used for the blowdown and evacuation steps. The exit flow rates were measured by two separate flow meters for the blowdown and evacuation steps. The flow meters were located as close as possible to the vacuum pumps. Two dedicated power meters were used to continuously measure power consumptions of the two vacuum pumps, the only power consuming equipment in the unit. The solenoid valves located near the inlets and outlets of the columns were used to switch between the different steps in the cyclic experiments. All the solenoid valves, flow controllers and meters, pressure transducers, thermocouples and CO_2 analyzers were connected to a programmable logic controller (PLC) manufactured by General Electric Corporation for implementing the cyclic operation, controlling the set points and measuring the process variables.

Error Analysis of Pilot Plant Data

The instrument specifications are listed along with the schematic in Figure 3. The accuracies of various direct measurements are bound by the accuracies of the measuring instruments.

The readings from the 60th cycle from two VSA experiments with identical operating conditions were compared to obtain the differences between various measured profiles. The differences in the collected sensor readings versus time data were subjected to *t*-tests. For all the sensor readings, *t* values were less than $t_{0.05}$, confirming good reproducibility of the experimental runs.

Experimental error bars for various performance indicators, namely purity, recovery, energy consumption, and productivity, were computed with readings from multiple sensors. The error bars were established by recalculating the performance indicators using expected upper and lower bounds of the readings from the various sensors based on their accuracies reported by the manufacturers. The range of errors thus

Table 2. Summary of the VSA Experiments Conducted at the Pilot Plant

Exp	t_{press} (s)	t_{ads} (s)	t_{bd} (s)	t_{evac} (s)	P_I (bar)	P_L (bar)	Purity (%)		Recovery (%)		Productivity (tonne CO_2/m^3 adsorbent/day)		Energy (kWh/tonne CO_2)		
							Exp	Theo	Exp	Theo	Exp	Theo	Exp	$\eta = 72\%$	$\eta = 30\%$
1+	20	60	150	310	0.070	0.025	94.7 ± 1.05	97.6	85.4 ± 4.52	86.2	1.40 ± 0.07	1.31	510.5 ± 25.5	173.9	417.4
2	20	20	150	310	0.072	0.009	85.1 ± 1.01	88.6	93.1 ± 4.83	94.2	0.87 ± 0.05	0.80	582.7 ± 39.4	278.5	668.4
3	20	40	150	310	0.072	0.021	94.5 ± 1.01	95.6	85.8 ± 5.01	84.8	1.18 ± 0.06	1.05	339.2 ± 23.6	190.3	456.7
4	20	40	150	310	0.192	0.022	83.4 ± 1.03	83.7	94.5 ± 5.92	95.6	1.24 ± 0.06	1.12	459.0 ± 31.9	192.0	460.8
5	20	40	150	310	0.052	0.011	95.9 ± 0.98	97.9	86.4 ± 5.90	80.6	1.17 ± 0.06	1.04	472.2 ± 45.4	201.6	483.8
6	40	60	150	310	0.071	0.023	92.9 ± 1.01	95.9	93.3 ± 7.07	94.0	1.27 ± 0.08	1.00	469.0 ± 30.4	189.7	455.3
7	40	60	150	310	0.056	0.022	94.8 ± 1.04	97.0	89.7 ± 7.13	93.3	1.17 ± 0.11	0.95	475.0 ± 46.6	191.5	459.6
8	40	60	150	310	0.043	0.022	96.3 ± 1.02	98.8	86.5 ± 4.07	90.3	1.15 ± 0.05	0.94	508.3 ± 50.8	204.1	489.8
Mean of absolute difference between model prediction and experimental result normalized with model prediction (%)							2.3		2.55		15.46			137.33	9.22
Standard deviation							1.06		2.17		7.06			31.24	9.25

The calculated error bars for the performance indicators are also included. "+" denotes the run chosen as the base case for LPP. Runs 1–3: Effect of adsorption step duration, Runs 3–5: effect of blowdown pressure, Runs 6–8: four-step with LPP. P_H = 1.5 bar for all cases. Note that the purity, recovery, and energy consumption values are represented up to one decimal place, and productivity up to two decimal places.

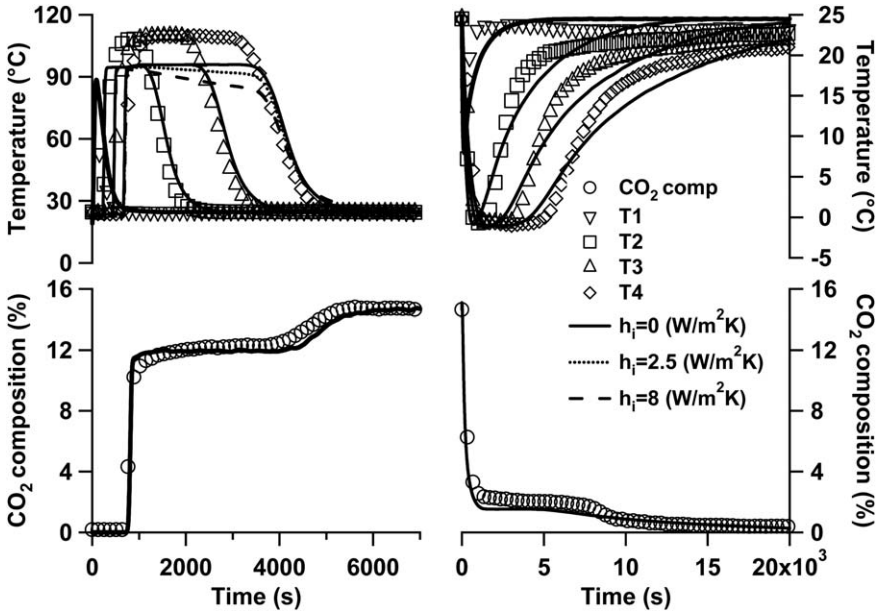

Figure 4. Adsorption and desorption profiles in a binary breakthrough experiment.

The lines denote model predictions.

calculated were $\sim\pm1\%$ for purity, ±4–7% for recovery, ±0.05–0.11 tonne CO_2 m^{-3} adsorbent day^{-1} for productivity, and ±23.6–50.8 kWh $tonne^{-1}$ CO_2 for energy consumption. The exact values are reported in Table 2 where the pilot plant runs have been compiled. The averages of these exact values, $\pm5.6\%$ for recovery, ±0.07 tonne CO_2 m^{-3} adsorbent day^{-1}, and ±36.7 kWh $tonne^{-1}$ CO_2 for energy consumption, are used when the results are discussed in later sections.

Modeling and Simulation of the Pilot Plant Experiments

Modeling and simulation of the pilot plant breakthrough and cyclic experiments were based on the nonisothermal, nonisobaric model presented by Haghpanah et al.[27] The model equations consisted of component and total mass balances, column and wall energy balance equations, and mass transfer rate equations. The pressure drop across the column was described by Darcy's equation. Linear driving force (LDF) approximation was used to describe the transport between gas and solid phases.[28] The model equations were discretized in space by WENO finite volume technique and the coupled ordinary differential equations (ODEs) were solved in MATLAB using stiff ODE solver ode23s and 30 finite volume elements were used for discretization. The model equations and the finite volume numerical scheme are provided in the Supplementary Information.

DCB Study

The column was packed with the adsorbent using a powder flex unit (Dietrich powder flex 100) which helped maintain a uniform distribution of the adsorbent in the column. After packing, the column was regenerated in a specially designed facility at 350°C for 8–10 h. To avoid heat loss and obtain a uniform temperature along the length of the column during regeneration, the column was insulated with 2 in.-thick glass wool pads. The column was subsequently cooled to ambient temperature, mounted onto the skid, and connected to the feed and product lines by flexible hoses. Adsorption breakthrough experiments were carried out by first saturating the column with pure N_2 and then introducing a feed containing 15% CO_2 and 85% N_2. Once the breakthrough was complete, desorption was started by switching back to pure nitrogen flow. The total inlet flow rate in all the breakthrough runs was kept at 1000 SLPM. It should be noted that thermal regeneration was carried out only once during the entire period of operation that lasted for 15 months and the column was regenerated by nitrogen purge for 12–15 h before each experiment.

Breakthrough experiments were carried out in both the columns and the results of these runs are discussed in this section. Figure 4 shows representative breakthrough curves from Column 1. The long plateaus at thermocouples T2–T4 clearly indicated that the column diameter was large enough to attain adiabatic behavior. Any significant heat loss from the columns in the radial direction would prevent the formation of such temperature plateaus. The temperature plateaus reached close to 110°C during adsorption and 0°C during desorption, which are expected due to the high enthalpy for CO_2 adsorption on zeolite 13X. The lower temperature rise recorded by the first thermocouple, T1, was most likely due to the influence of the distributor plate, which was only 0.043 m away. The CO_2 composition measured at the column outlet shows two transitions. The first transition around 600 s, a sharp jump from 0 to 12 mol % CO_2, was a consequence of the adiabatic thermal front. The second transition around 4000 s, a gradual transition from 12 to 15 mol % CO_2, corresponded to the complete elution of the thermal front from the adiabatic plateau back to the initial temperature. Consequently, the second transition closely followed the drop in the temperature of the 4th thermocouple, T4, which was nearest to the column exit where the CO_2 concentration was monitored.

The results from the simulation are shown along with the experimental profiles in Figure 4. It is worth noting that the simulations are fully predictive using single component equilibrium data obtained from the gravimetric balance (that

used ~1 g of the adsorbent) and by assuming macropore molecular diffusion controlled mass transfer rate. The simulation was able to capture the breakthrough time and the transitions in the composition and temperature profiles. The maximum (plateau) temperature reached in the experiment was however higher than that attained in the simulation. This was consistently seen in all the breakthrough runs. Parameter tuning to compensate for suspected underestimation of heat of adsorption or overestimation of adsorbent heat capacity were able to increase the predicted plateau temperature, but at the expense of losing the agreements with the transitions. Given the good matches with all other key features of the breakthrough profiles, the mismatch in the maximum temperature is somewhat intriguing. As already mentioned, any significant heat loss from the columns in the radial direction would prevent the formation of the temperature plateaus. This is evident from the profiles of T4 in Figure 4, where it is shown that the temperature plateau is not obtained from simulation even for a small nonzero inside heat-transfer coefficient (h_i) of 2.5 W m^{-2} K.

Two breakthrough experiments, performed 10 months apart in Column 1, gave nearly identical responses (see Figure S3 in Supplementary Information), thereby, confirming that the adsorbent capacity was unaffected after repeated cycling, and the method adopted to regenerate the adsorbent between the runs, a combination of nitrogen purge and pulling vacuum, was indeed effective. The breakthrough results from Column 1 and Column 2, conducted under very similar conditions, were also compared. Like in the previous case, the breakthrough experiments showed good reproducibility (see Figure S4 in the Supplementary Information). Therefore, the two columns were considered to be identical and suitable for performing VSA process experiments involving coupled steps, which are discussed later.

Cyclic Experiments

Basic four-step VSA

After the breakthrough experiments, the next step was to explore VSA cycles. In a previous publication, we reported a detailed theoretical study of a simple four-step VSA process consisting of pressurization, high pressure adsorption, forward blowdown, and reverse evacuation.[9] It was shown that it is possible to exploit the high selectivity of zeolite 13X using this rather simple cycle to obtain high purity and recovery. In this section, the experimental implementation of this process is described. The four-step cycle shown in Figure 5a comprised of the following steps:

1. Pressurization: in this step, the column, which was initially at vacuum, was pressurized to a high pressure, P_H, by introducing the feed at a predetermined rate from the feed end with the other end of the column closed.

2. High pressure adsorption: the column was continuously fed at the same rate, but the product end was now opened. CO_2 was preferentially adsorbed, while nitrogen product was withdrawn from the product end.

3. Forward blowdown: in this step, the feed end was closed while the column was depressurized to an intermediate pressure, P_I, from the product end. The main purpose of this forward blowdown step was to remove as much nitrogen as possible from the column while conserving CO_2 as much as possible to obtain CO_2 with high purity and recovery from the evacuation step.

4. Reverse evacuation: the column was evacuated to a low pressure, P_L, in the reverse direction from the feed end to recover the adsorbed CO_2.

The advantage of the above uncoupled steps is that the cycle can be implemented in a single bed. However, a single bed implementation cannot take in continuous feed.

Prior to any experiment, the column was purged with N_2 overnight for 12–15 h. It was then evacuated to a low pressure (0.02 bar). The durations of each step, flow rates, intermediate pressure (P_I), number of cycles, and the operating sequence of the solenoid valves were fed as inputs to the PLC and the entire process was operated in an automatic mode. The process was run for 300 cycles to ensure cyclic steady state (CSS) was reached. During this period, the exit CO_2 compositions, temperatures at four different locations along the column, inlet and exit pressures, and exit flow rates were continuously logged using the Intouch Wonderware software.

In the VSA runs, the adsorption step operated at a pressure of 1.5 bars. In all the runs, the pressurization time was kept constant at 20 s. Any duration less than 20 s is not easy to implement using solenoid valves, while longer durations did not have any significant impact on the performance of the process.[9]

Five basic four-step VSA runs were carried out, which are detailed in Table 2. Figures 6–8 show variations of the different measured variables with cycle number for a representative Run 1 in Table 2. The CO_2 composition profiles during high pressure adsorption, forward blowdown, and reverse evacuation steps are shown in Figure 6. These profiles indicate that there were significant CO_2 losses in the adsorption and the blowdown steps and the CO_2 concentration in the evacuation step was more than 90%. The transient temperature profiles shown in Figure 8 clearly indicate the progress of the thermal front during the cycles. The temperature swings in the thermocouples T1 and T2 were much higher than those in T3 and T4, indicating that the CO_2 adsorption and desorption, were primarily confined in the first half of the bed, while the rest of the bed mostly had adsorption and desorption of nitrogen. The rise and fall of the mean temperature levels at T2 to T4 in sequence before coming to CSS further suggest that there was a net progress of the thermal front in the direction of the feed flow. This is expected because there was net accumulation of CO_2 in the early cycles before reaching CSS, when adsorption and desorption amounts became equal.

In the basic four-step VSA process simulations, the bed was initially assumed to be saturated with the light component at low pressure (P_L) at the average of the temperatures recorded by the four thermocouples at the end of nitrogen purge for the run under consideration. In the first step, that is, pressurization, the inlet pressure profile with time was provided as the input and the pressure across the column was calculated from the total mass balance. The inlet velocity was obtained from the Darcy's equation and the exit velocity was kept zero. In the adsorption step, the inlet velocity and the exit pressure were provided as the inputs. For the blowdown and evacuation steps, which involved depressurization to different vacuum levels, the pressure profiles at the open ends were provided as exponential functions, with the exponential time constant tuned to match the measured pressure profiles in the pilot plant. The final conditions of each step were taken as the initial conditions of the subsequent step. To be consistent with the experimental runs, the VSA processes were simulated for 300 cycles and the transients of the 300th cycle were used to calculate CO_2 purity, recovery, and productivity, and energy consumption of the process.

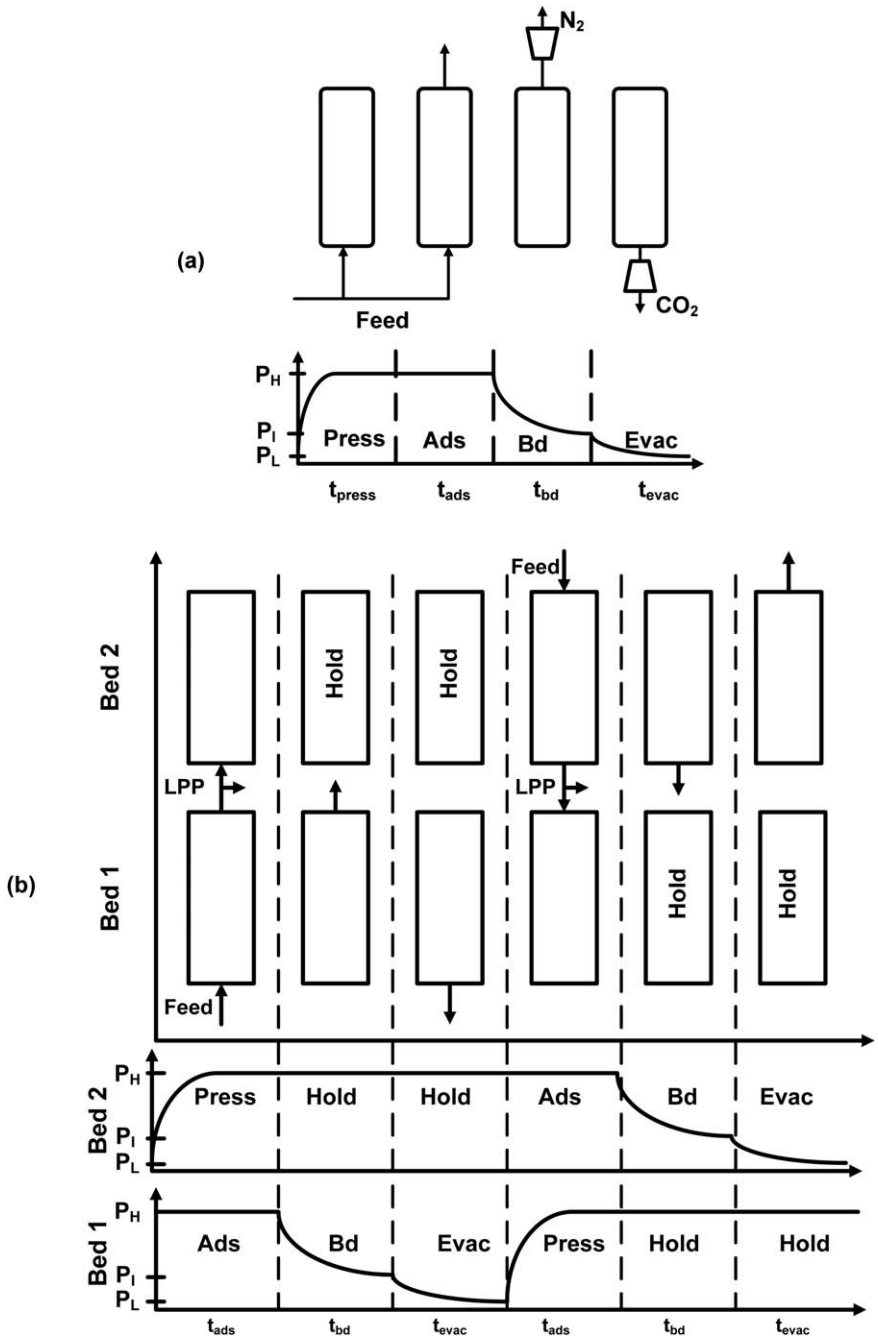

Figure 5. (a) Basic four-step VSA and (b) four-step VSA with light product pressurization.

P_H—high pressure, P_I—blowdown pressure, P_L—evacuation pressure, t_{ads}—adsorption time, t_{bd}—blowdown time, and t_{evac}—evacuation time.

The computed (model predictions) transient profiles of composition, pressure, flow rate, and temperature profiles for Run 1 in Table 2 are included in Figures 6–8. The predicted trends were generally in good agreement with the profiles measured in the pilot plant. From Figure 8, it can be seen that except for the first thermocouple, the maximum values attained in the simulation at the other thermocouples were lower than those obtained in the experiment. These trends are similar to those observed in the breakthrough experiments discussed earlier. However, the predicted swings as well as the mean temperature levels were generally somewhat higher than those in the experiment. The net progress of the thermal front in the direction of the feed flow, evident from the rise and fall of the mean temperature levels at T2 to T4 in sequence before coming to the CSS, was also somewhat faster in the simulation than in the actual run. On the other hand, in the breakthrough runs, the experimental and computed transitions in the temperature profiles were in good agreement, which was an indication that the thermal wave velocity was correctly calculated in the breakthrough simulation. The mismatch in case of the VSA runs most likely arises from not fully capturing the dynamics of rapid pressurization from low vacuum pressure to atmospheric pressure at the entrance of the bed. Despite the small quantitative differences, the overall qualitative features of the four thermocouple readings observed experimentally were correctly captured in the computed profiles. The

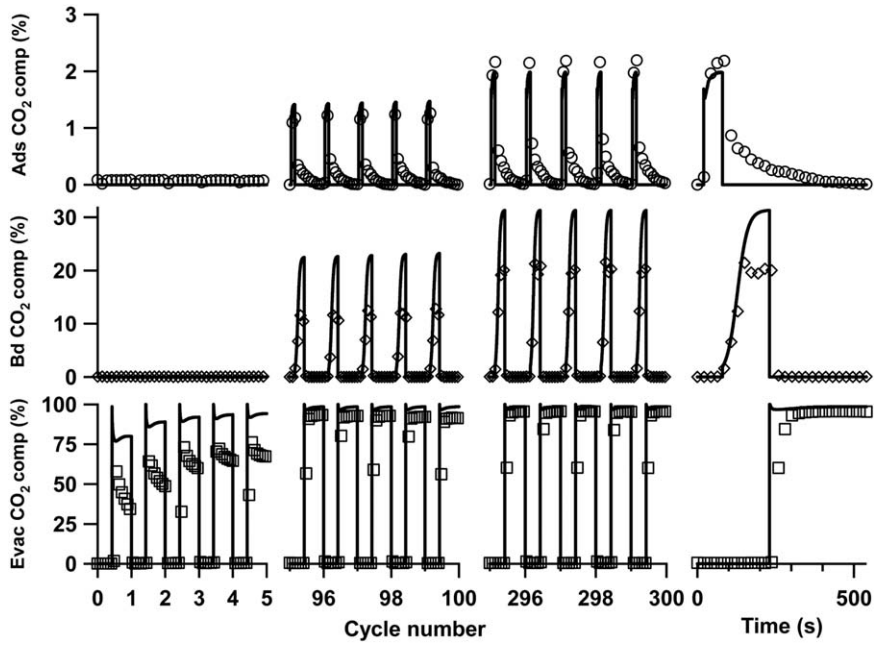

Figure 6. Transient CO_2 composition profiles for VSA experiment Run 1 in Table 2.

The symbols are experimental results and the lines denote model predictions. Ads, Bd, and Evac stand for adsorption, blowdown, and evacuation, respectively.

computed temperature profiles also showed lower temperature swings in thermocouples 3 and 4, which, as mentioned earlier, indicated that these zones of the bed were mainly undergoing adsorption/desorption of nitrogen and CO_2 concentration front was confined in the first half of the bed. Better bed utilization was not possible due to the tail that developed from the unfavorable desorption of the strongly favorable CO_2 equilibrium isotherm.

The effects of adsorption step duration and the blowdown pressure on purity and recovery were also studied and these results are presented in Figure 9. As shown in Figure 9a, with an increase in the adsorption step time, there was an improvement in purity while the recovery decreased. This was due to the fact that with increase in the adsorption time, the CO_2 front moved further into the column resulting in more losses in the effluents from the high pressure adsorption and blowdown steps. Therefore, in our experiments, when the adsorption time was increased from 20 to 40 s, the purity improved from 85.1 ± 1 to $94.5 \pm 1\%$, while the recovery dropped from 93.1 ± 5.6 to $85.8 \pm 5.6\%$. Further

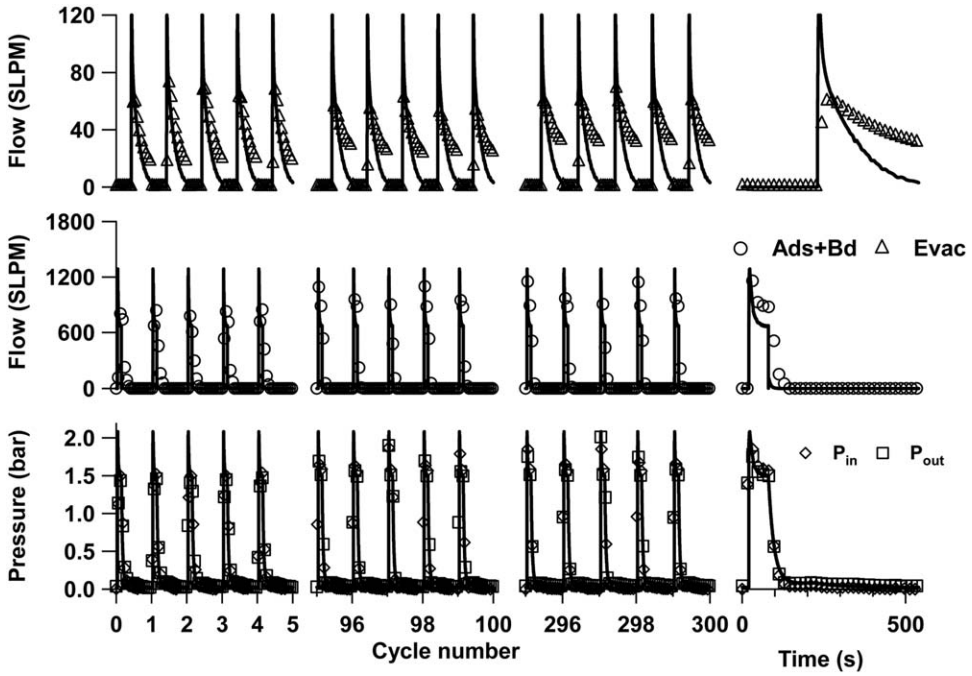

Figure 7. Transient pressure and flow profiles for VSA experiment Run 1 in Table 2.

The symbols are experimental results and the lines denote model predictions. Ads, Bd, and Evac stand for adsorption, blowdown, and evacuation, respectively. P_{in} and P_{out} are pressures at the feed and the light product ends, respectively.

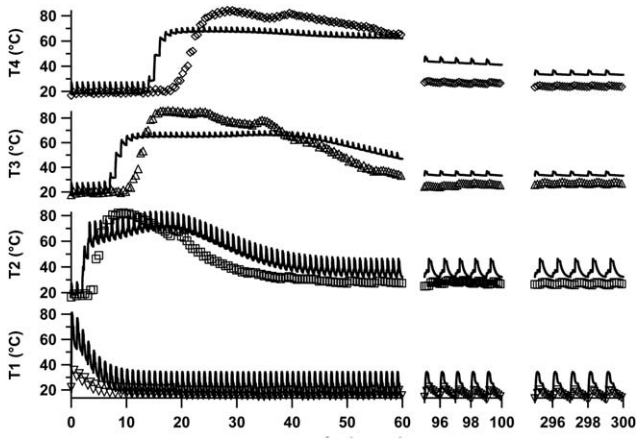

Figure 8. Transient temperature profiles for VSA experiment Run 1 in Table 2.

The lines denote model predictions.

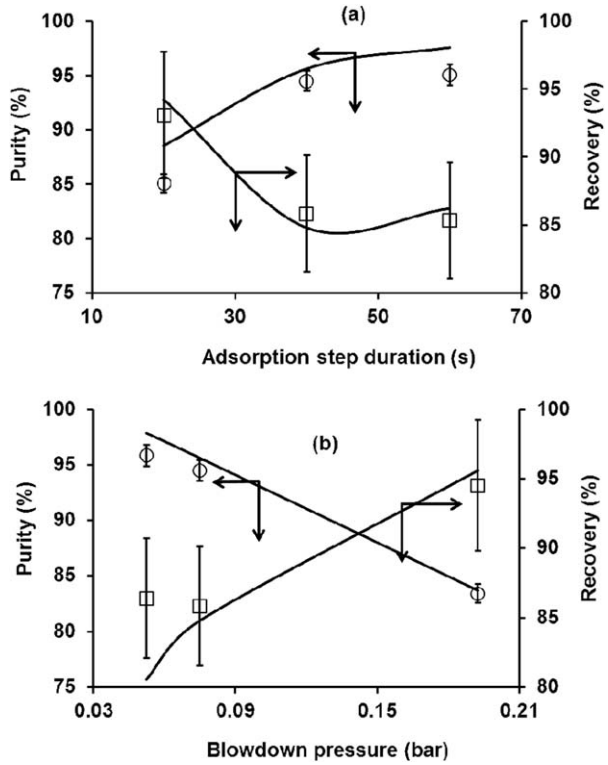

Figure 9. Effect of (a) adsorption step duration and (b) blowdown step pressure.

The lines denote model predictions.

increase in the adsorption time to 60 s improved the purity to $94.7 \pm 1\%$ with a small drop in recovery.

It was earlier mentioned that the main purpose of the blowdown step was to remove the nitrogen from the product end to recover CO_2 in high purity in the evacuation step. With an increase in the blowdown pressure, the purity decreased and recovery increased (see Figure 9b). At higher blowdown pressures, nitrogen was not sufficiently removed from the column and hence the CO_2 was recovered in the evacuation step at a lower purity. Higher blowdown pressure also meant lower CO_2 loss, which explains the increase in recovery. In our study, we analyzed three blowdown step pressures, viz. 0.052, 0.072, and 0.192 bar and the results are shown in Figure 9b. When the pressure was increased from 0.072 to 0.192 bar, the purity dropped from $94.5 \pm 1\%$ to $83.4 \pm 1\%$, while the recovery improved from $85.8 \pm 5.6\%$ to $94.5 \pm 5.6\%$. By further reducing the pressure from 0.072 to 0.052 bar, the purity increased to around $95.9 \pm 1\%$ while the recovery remained around $86.4 \pm 5.6\%$.

The model predictions shown in Figure 9 are in good agreement with the experimental trends. Detailed comparison of all the performance indicators, namely, purity, recovery, energy consumption, and productivity for all the basic four-step runs are also included in Table 2 along with the ranges of errors for the experimental values. The extents of quantitative agreements between the experimental and theoretical values will be addressed after discussing the results from four-step VSA process with LPP.

Four-step VSA with LPP

In the basic four-step VSA process, CO_2 losses with the nitrogen product in the high pressure adsorption step and in the effluent from the blowdown step affect its recovery. It is therefore essential to minimize the CO_2 loss from these two steps without compromising nitrogen removal, which controls CO_2 product purity. One way to achieve this is to pressurize the bed with the light product from the product end to recycle the CO_2, which would otherwise be lost with the nitrogen product. However, nitrogen that is recycled, if not adequately removed in the blowdown step, will contaminate the CO_2 product from the evacuation step and reduce its purity. Haghpanah et al.[27] have shown using detailed simulations that LPP sharpens the CO_2 concentration front in the bed. As a result, compared to the basic four-step cycle, the blowdown step can be executed at a lower P_I to remove the excess nitrogen recycled with CO_2 without sacrificing the increased recovery benefit from the recycled CO_2. Thus, the four-step VSA with LPP increases both purity and recovery compared to the basic four-step cycle. Following a rigorous energy-productivity optimization subject to purity-recovery constraints, Haghpanah et al.[27] further showed that the four-step cycle with LPP was the most energy efficient cycle amongst the six cycle configurations investigated. Therefore, the four-step VSA with LPP was included in the pilot plant study.

In the pilot plant, the four-step VSA cycle with LPP was implemented by using two adsorption columns with appropriately inserted idle/hold steps, as shown in Figure 5b. The exit stream during high pressure adsorption step from Column 1 was used to pressurize Column 2. After the high pressure adsorption step, blowdown and evacuation steps were carried out in the former while the latter remained idle. Subsequently, these steps were carried out in Column 2 and Column 1 remained idle for some time after pressurization with the light product from Column 2. Similar to the basic four-step VSA experiment, the LPP runs were also carried out for 300 cycles to ensure CSS. The LPP runs are also summarized in Table 2.

To experimentally validate the performance improvement of the four-step cycle with LPP over the basic four-step cycle, we chose Run 1 in Table 1, which had significant CO_2 losses in the adsorption and blowdown steps, as the base case. The CO_2 composition profiles in the adsorption and blowdown steps from this run are compared with two LPP Runs 6 and 7 in Figures 10a, b. Besides the pressurization time, all other operating conditions for Runs 1, 6, and 7

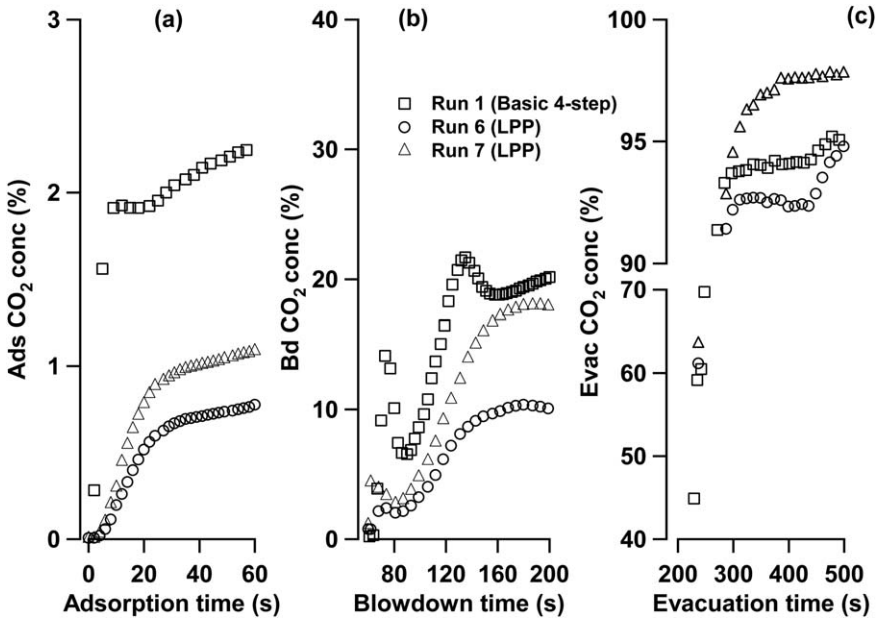

Figure 10. CO_2 concentration profiles in (a) adsorption step (b) blowdown step, and (c) evacuation step in basic four-step VSA Run 1 and LPP Runs 6 and 7.

Ads, Bd, and Evac represent adsorption, blowdown, and evacuation steps, respectively. The symbols have the same meanings in all three parts of the figure.

were the same. The pressurization time in the basic four-step VSA process was kept fixed at 20 s. However, in case of LPP, longer duration (40 s) was needed to pressurize the bed with the product from the high pressure adsorption step in the other bed. Longer pressurization time did not have any impact of the performance of the basic four-step cycle. Hence, the difference in pressurization times of the two cycles was not consequential. It is clear that the CO_2 losses in Run 6 were much lower compared to those in Run 1, thus confirming the recovery benefit of the LPP cycle. However, the CO_2 concentration in the evacuation step was lower in Run 6 compared to Run 1, as shown in Figure 10c. By lowering the blowdown pressure, the loss in CO_2 purity was more than compensated which is also seen from Figure 10c.

The actual purity-recovery values from the LPP cycle are compared with those from the basic four-step cycle in Figure 11. As seen from the figure, under similar conditions of $P_I = 0.07$ bar, the LPP experiment had a much higher recovery ($93.3 \pm 5.6\%$ versus $85.4 \pm 5.6\%$) but a lower purity ($92.9 \pm 1\%$ versus $94.7 \pm 1\%$). This is due to the contamination of the CO_2 product by the nitrogen, which was used to pressurize the bed. The loss in purity was recovered by slightly lowering the blowdown pressure to 0.056 bar to remove sufficient amount of nitrogen. The recovery of CO_2 reduced slightly but was still higher than the CO_2 recovery obtained from the basic four-step. Further reduction in the blowdown pressure to 0.043 bar improved the purity to $96.3 \pm 1\%$, while the recovery was $86.5 \pm 5.6\%$.

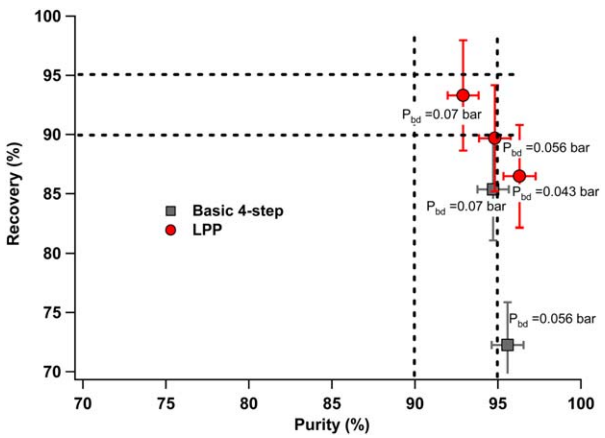

Figure 11. Demonstration of improvement in purity and recovery by incorporating a LPP step.

[Color figure can be viewed in the online issue, which is available at wileyonlinelibrary.com.]

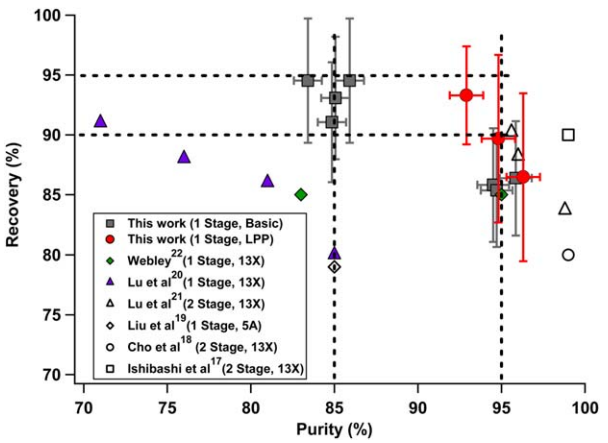

Figure 12. Comparison of experimentally achieved purity and recovery in this study with other pilot plant data reported in the literature.

The error bars are shown only for purity and recovery values from our pilot plant runs.

[Color figure can be viewed in the online issue, which is available at wileyonlinelibrary.com.]

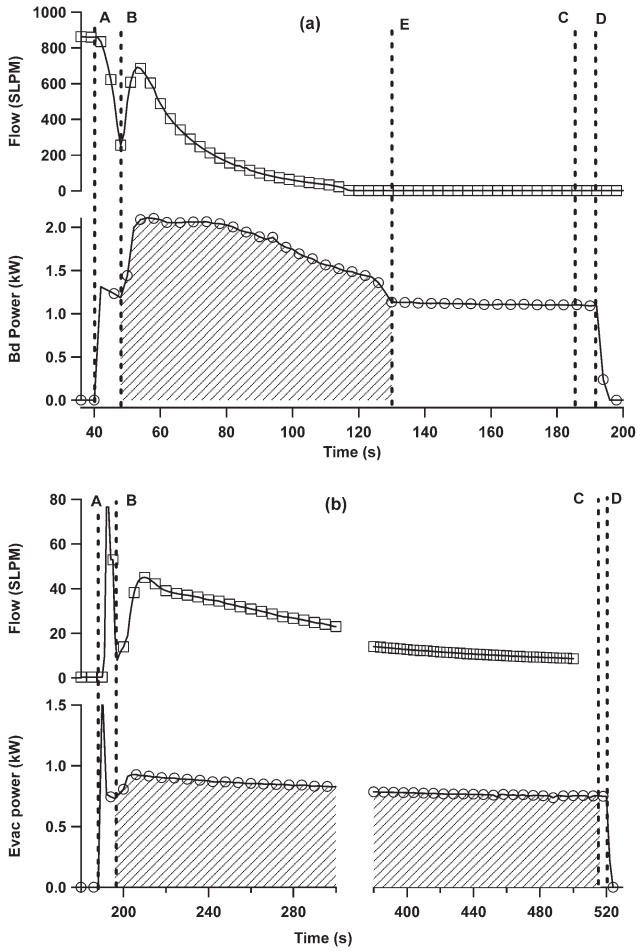

Figure 13. Power and flow rate measurements in (a) blowdown and (b) evacuation steps.

A: vacuum pump on, B: solenoid valve on, C: solenoid valve off, D: vacuum pump off E: zero flow.

The purity-recovery values obtained from the pilot plant experiments are compared with the values reported in the literature[17–22] in Figure 12. Clearly, our pilot plant was able to achieve $94.8 \pm 1\%$ purity and $89.7 \pm 5.6\%$ recovery in a single stage. These are very close to the 95% purity and 90% recovery requirements specified by the US Department of Energy.

In the present study, the productivity values for all pilot plant runs were in the range $0.87–1.4 \pm 0.07$ tonnes CO_2 m^{-3} adsorbent day^{-1}. The mean and standard deviation values for the absolute percentage differences between the model predictions and experimental results normalized with respect to the former are also given in Table 2 for all the performance indicators. The overall quantitative agreements between the experimental and theoretical purity and recovery were satisfactory, as suggested by the low values of mean and standard deviation. These values were relatively higher for productivity indicating modest agreements between experimental values and model predictions. The deviations for energy consumption were exceptionally large, which is discussed next.

Energy consumption in a cyclic VSA process

As the high pressure steps were operated around atmospheric pressure, the energy consumption in our pilot plant VSA experiments came from the blowdown and the evacuation steps. The power consumed by the vacuum pumps in these two steps was measured directly with power meters. The readings from the power meters are plotted along with the flow rates in Figure 13. The initial rise in the power meter readings corresponds to the time when the vacuum pump was turned on (position A). There was some degree of overshoot, which settled over the next couple of seconds till the solenoid valves were turned on, indicated by position B. Once the solenoid valves were turned on, the vacuum pumps started to receive flow and this increased in the power meter readings. The flow rate decreased with time and this effect was also seen in the power profiles. The solenoid valves were closed a few seconds before the vacuum pumps. Closing of solenoid valves and vacuum pumps are indicated by positions C and D, respectively. The readings became zero once the vacuum pump was turned off. However, in case of the blowdown step, the flow ceased around 126 s, beyond which the vacuum pump was operating without receiving any gas from the column. This would not have happened if the variable speed pumps were used. This situation will also not arise in a continuous process, where the vacuum pumps will receive gas for the entire duration. Therefore, the true power consumed in the blowdown step is the area under the curve between positions B and E shown by shaded region. The total power consumption in a VSA process is the sum of the power consumptions in the blowdown and evacuation steps. The energy consumption values in the pilot plant experiments were in the range of $339–583 \pm 36.7$ kWh $tonne^{-1}$ of CO_2 captured. The power consumptions obtained from direct measurements are compared with the results obtained from conventional isentropic calculations in Figure 14. The commonly used efficiency in most published carbon capture studies based only on process simulation is 72%.[29,30] It can be seen that, with 72% efficiency, the theoretical power consumptions were considerably lower than the direct measurements from the experiments and a lower efficiency

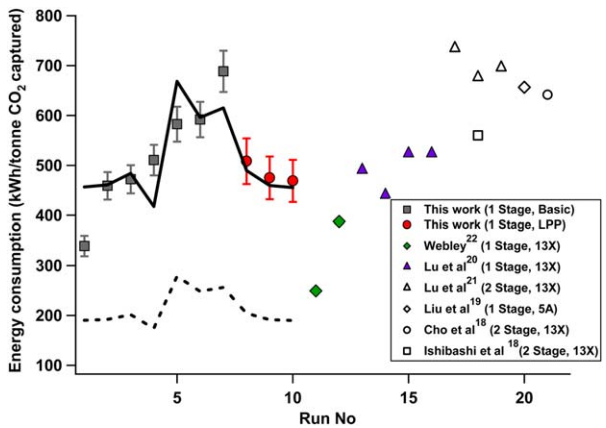

Figure 14. Comparison of Energy consumption values from our pilot plant experiments with other data in literature.

The dotted line denotes an efficiency of 72% while the solid line denotes an efficiency of 30%. Note that all the experiments, both from this work and from the literature, resulted in different purity-recovery values, and care should be taken in comparing their energy consumptions. [Color figure can be viewed in the online issue, which is available at wileyonlinelibrary.com.]

of 30% was found to match the experimental power consumptions for all the runs. As shown in Table 2, the mean of absolute % deviations between experimental and predicted results normalized with respect to the latter reduced from 137.33% at 72% efficiency to 9.22% at 30% efficiency. The power consumptions from our experiments are of similar orders of magnitude to those in the literature[17–22] obtained from similar direct measurements and these are also shown in Figure 14. We are unable to calculate the efficiencies for the published power consumption values due to lack of necessary details. But comparable magnitude of measured power may imply that the efficiencies could be much lower than 72%, as observed in our runs. In fact, 72% efficiency is representative of typical compressors, but reported efficiencies are in the range 50–70% for typical vacuum systems based on hydrocarbon data.[31] Our measured value of 30% is the first reported for a CO_2 evacuation.

Conclusions

The capture of CO_2 from a dry flue gas was demonstrated on a pilot plant scale. Column breakthrough experiments were conducted first and the temperature profiles in these experiments showed long plateaus, typical of an adiabatic column. Basic four-step VSA experiments were then conducted using a single column in the pilot plant. The effects of adsorption step duration and blowdown step pressures were studied. Further, four-step VSA experiments with LPP step were conducted and these experiments showed significant improvement in recovery compared to the basic four-step VSA experiments. The pilot plant experiments were then used to validate a nonisothermal nonisobaric model and in general, good agreement between the experiment and theory was observed. Next, the energy consumption values obtained from direct measurements in our pilot plant were compared with theoretical isentropic calculations and it was found that an efficiency factor of 30% best described our pilot plant energy consumption values. The best performance achieved for the basic four-step VSA cycle was $95.9 \pm 1\%$ purity, $86.4 \pm 5.6\%$ recovery with a productivity of 1.17 ± 0.07 tonne CO_2 m^{-3} adsorbent day^{-1} and an energy consumption of 472.2 ± 36.7 kWh $tonne^{-1}$ CO_2. In case of LPP, $94.8 \pm 1\%$ purity and $89.7 \pm 7\%$ recovery were achieved with a productivity of 1.17 ± 0.07 tonne CO_2 m^{-3} adsorbent day^{-1} and an energy consumption of 475 ± 36.7 kWh $tonne^{-1}$ CO_2. The higher error bars for the recovery is due to the lower flow rates during the evacuation step. This is the first pilot plant study in which nearly 95% purity and 90% recovery were achieved in a single stage.

The present study is based on dry flue gas and it does not address the process economics. Effect of moisture and costing are important issues. However, these issues are research topics in their own right and merit-independent attention. Detailed studies are in progress on carbon capture from wet flue gas and costing of a large-scale adsorption-based capture process. These two studies in progress will be communicated in due course.

Acknowledgments

Financial support from the A*STAR grant on Carbon capture and utilization—Thematic strategic research program (CCU-TSRP) is acknowledged. We acknowledge Zeochem for providing the adsorbent used in the pilot plant.

Notation

b = pre-exponential constant for site 1 in dual-site Langmuir isotherm, m^{-3} mol
c = gas phase composition, mol m^{-3}
d = pre-exponential constant for site 2 in dual-site Langmuir isotherm, m^{-3} mol
P = pressure, bar
q^* = equilibrium loading, mol m^{-3}
q_{sb} = saturation constant for site 1 in dual-site Langmuir model, mol m^{-3}
q_{sd} = saturation constant for site 2 in dual-site Langmuir model, mol m^{-3}
R = universal gas constant, J mol^{-1} K^{-1}
T = temperature, K
U = internal energy, J mol^{-1}

Subscripts

0 = pre exponential constant
b = site 1 in dual-site Langmuir isotherm
d = site 2 in dual-site Langmuir isotherm
H = high pressure
I = intermediate pressure
i = component
L = low pressure

Literature Cited

1. IPCC Special Report. Carbon dioxide capture and storage. In: *IPCC Special Report, Prepared by Working Group III of the Intergovernmental Panel on Climate Change, Bert Metz, Ogunlade Davidson,* Heleen de conninck, Manuela Loos, Leo de Meyer, Editors. New York: Cambridge University Press, 2005.
2. Haszeldine RS. Carbon capture and storage: how green can black be? *Science*. 2009;325(5948):1647–1652.
3. Report of DOE NETL, Office of Program Planning and Analysis. Quality guidelines for energy system studies, CO_2 impurity design parameters, DOE-NETL, Jan. 2012.
4. Bhown AS, Freeman BC. Analysis and status of post-combustion carbon dioxide capture technologies. *Env Sci Tech.* 2011;45(20): 8624–8632.
5. Steeneveldt R, Berger B, Torp T. CO_2 Capture and storage: closing the Knowing–Doing Gap. *Chem Eng Res Des.* 2006;84(9):739–763.
6. Davison J, Thambimuthu K. Technologies for capture of carbon dioxide, *Greenhouse Gas Control Technol.* 2005;7:3–13.
7. Aaron D, Tsouris C. Separation of CO_2 from Flue Gas: a review. *Sep Sci Technol.* 2005;40(1):321–348.
8. Zhang J, Webley P, Xiao P. Effect of process parameters on power requirements of vacuum swing adsorption technology for CO_2 capture from flue gas. *Energy Convers Manage.* 2008;49(2): 346–356.
9. Haghpanah R, Majumder A, Nilam R, Rajendran A, Farooq S, Karimi IA. Multiobjective optimization of a four-step adsorption process for postcombustion CO_2 capture via finite volume simulation. *Ind Eng Chem Res.* 2013;52(11):4249–4265.
10. Farooq S, Ruthven DM. Numerical simulation of a kinetically controlled pressure swing adsorption bulk separation process based on a diffusion model. *Chem Eng Sci.* 1991;46(9):2213–2224.
11. Wilson SJ, Beh CCK, Webley PA, Todd RS. The effects of a readily adsorbed trace component (water) in a bulk separation PSA process: the case of oxygen VSA. *Ind Eng Chem Res.* 2001;40(12): 2702–2713.
12. Malek A, Farooq S. Hydrogen purification from refinery fuel gas by pressure swing adsorption. *AIChE J.* 1998;44(9):1985–1992.
13. Sircar S, Golden TC. Purification of hydrogen by pressure swing adsorption. *Sep Sci Technol.* 2000;35(5):667–687.
14. Grande CA, Rodrigues AE. Propane/propylene separation by Pressure Swing Adsorption using zeolite 4A. *Ind Eng Chem Res.* 2005; 44(23):8815–8829.
15. Ritter JA, Yang RT. Pressure swing adsorption: experimental and theoretical study on air purification and vapor recovery. *Ind Eng Chem Res.* 1991;30(5):1023–1032.

16. Ebner AD, Ritter JA. State-of-the-art adsorption and membrane separation processes for carbon dioxide production from carbon dioxide emitting industries. *Sep Sci Technol*. 2009;44(6):1273–1421.
17. Ishibashi M, Ota H, Akutsu N, Umeda S, Tajika M, Izumi J, Yasutake A, Kabata T, Kageyama Y. Technology for removing carbon dioxide from power plant flue gas by the physical adsorption method. *Energy Convers Manage*. 1996;37(6–8):929–933.
18. Cho S-H, Park J-H, Beum H-T, Han S-S, Kim J-N. A 2-stage psa process for the recovery of CO_2 from flue gas and its power consumption. *Stud Surf Sci Catal*. 2004;153:405–410.
19. Liu Z, Wang L, Kong X, Li P, Yu J, Rodrigues AE. Onsite CO_2 capture from flue gas by an adsorption process in a coal-fired power plant. *Ind Eng Chem Res*. 2012;51(21):7355–7363.
20. Lu W, Ying Y, Shen W, Li P, Yu J. CO_2 capture from flue gas in an existing coal power plant. In: 6th Pacific Basin Conference on Adsorption Science and Technology, Baltimore, MD, 2013.
21. Lu W, Ying Y, Shen W, Li P, Yu J. Experimental evaluation on CO2 capture from flue gas by two successive VPSA units in an existing coal power plant. In: 11th International Conference on Fundamentals of Adsorption, Baltimore, MD, 2013.
22. Webley PA. Adsorption processes for CO_2 separation. In: *11th International Conference on Fundamentals of Adsorption*, Baltimore, MD, 2013.
23. Xiao P, Zhang J, Webley P, Li G, Singh R, Todd R. Capture of CO_2 from flue gas streams with zeolite 13X by vacuum-pressure swing adsorption. *Adsorption*. 2008;14(4-5):575–582.
24. Ritter JA, Bhadra SJ, Ebner AD. On the use of the dual-process langmuir model for correlating unary equilibria and predicting mixed-gas adsorption equilibria. *Langmuir*. 2011;27(8):4700–4712.
25. Hu X, Mangano E, Friedrich D, Ahn H, Brandani S. Diffusion mechanism of CO_2 in 13X zeolite beads. *Adsorption*. 2013;20(1):121–135.
26. Giesy TJ, Wang Y, Levan MD. Measurement of mass transfer rates in adsorbents: new combined-technique frequency response apparatus and application to CO_2 in 13X zeolite. *Ind Eng Chem Res*. 2012; 51(35):11509–11517.
27. Haghpanah R, Nilam R, Rajendran A, Farooq S, Karimi IA. Cycle synthesis and optimization of a VSA process for postcombustion CO_2 capture. *AIChE J*. 2013;59(12):4735–4757.
28. Glueckauf E. Theory of chromatography. Part 10 formula for diffusion into spheres and their application to chromatography. *Trans Far Soc*. 1955;51:1540–1951.
29. Agarwal A, Biegler LT, Zitney SE. A superstructure-based optimal synthesis of PSA cycles for post-combustion CO_2 capture. *AIChE J*. 2010;56(7):1813–1828.
30. Maring BJ, Webley PA. A new simplified pressure/vacuum swing adsorption model for rapid adsorbent screening for CO_2 capture applications. *Int J Greenhouse Gas Control*. 2013;15:16–31.
31. Ulrich GD, Vasudevan, PT. *Chemical Engineering: Process Design and Economics A Practical Guide*, *2nd ed*. New Hampshire: Process Publishing, 2004.

Manuscript received Aug. 17, 2013, and revision received Jan. 3, 2014.